Investigation of protein-protein interactions and hotspot region on the NSP7-NSP8 binding site in NSP12 of SARS-CoV-2

José Xavier Lima Neto[1], Katyanna Sales Bezerra[1], Emmanuel Duarte Barbosa[1], Roniel Lima Araujo[1], Douglas Soares Galvão[2], Marcelo Leite Lyra[3], Jonas Ivan Nobre Oliveira[1]*, Shopnil Akash[4], Yousef A. Bin Jardan[5], Hiba-Allah Nafidi[6], Mohammed Bourhia[7]* and Umberto Laino Fulco[1]

[1]Department of Biophysics and Pharmacology, Bioscience Center, Federal University of Rio Grande do Norte, Natal, Brazil, [2]Applied Physics Department, University of Campinas, Campinas, São Paulo, Brazil, [3]Physics Institute, Federal University of Alagoas, Maceió, Brazil, [4]Department of Pharmacy, Daffodil International University, Dhaka, Bangladesh, [5]Department of Pharmaceutics, College of Pharmacy, King Saud University, Riyadh, Saudi Arabia, [6]Department of Food Science, Faculty of Agricultural and Food Sciences, Laval University, Quebec City, QC, Canada, [7]Department of Chemistry and Biochemistry, Faculty of Medicine and Pharmacy, Ibn Zohr University, Laayoune, Morocco

Background: The RNA-dependent RNA polymerase (RdRp) complex, essential in viral transcription and replication, is a key target for antiviral therapeutics. The core unit of RdRp comprises the nonstructural protein NSP12, with NSP7 and two copies of NSP8 (NSP81 and NSP82) binding to NSP12 to enhance its affinity for viral RNA and polymerase activity. Notably, the interfaces between these subunits are highly conserved, simplifying the design of molecules that can disrupt their interaction.

Methods: We conducted a detailed quantum biochemical analysis to characterize the interactions within the NSP12-NSP7, NSP12-NSP81, and NSP12-NSP82 dimers. Our objective was to ascertain the contribution of individual amino acids to these protein-protein interactions, pinpointing hotspot regions crucial for complex stability.

Results: The analysis revealed that the NSP12-NSP81 complex possessed the highest total interaction energy (TIE), with 14 pairs of residues demonstrating significant energetic contributions. In contrast, the NSP12-NSP7 complex exhibited substantial interactions in 8 residue pairs, while the NSP12-NSP82 complex had only one pair showing notable interaction. The study highlighted the importance of hydrogen bonds and π-alkyl interactions in maintaining these complexes. Intriguingly, introducing the RNA sequence with Remdesivir into the complex resulted in negligible alterations in both interaction energy and geometric configuration.

Conclusion: Our comprehensive analysis of the RdRp complex at the protein-protein interface provides invaluable insights into interaction dynamics and

energetics. These findings can guide the design of small molecules or peptide/peptidomimetic ligands to disrupt these critical interactions, offering a strategic pathway for developing effective antiviral drugs.

1 Introduction

After the first report in December 2019, the COVID-19 pandemic has spread around the world, causing more than 767 million confirmed infections and almost 7 million deaths until July 2023 (World Health Organization, 2020). Despite the decrease in deaths after the beginning of the vaccination programs, the continuous mutation of the virus has reduced the protective efficacy of the available vaccines and monoclonal antibodies (mAbs) (Harvey et al., 2021; McCarthy et al., 2021; Cox et al., 2023). Moreover, only a few drugs have shown some degree of efficacy in treating the infection and its complications, with some of them being reported to present severe side effects, resistance, and rebound phenomena (Kobryn et al., 2021; Anderson et al., 2022; Charness et al., 2022; Zhai et al., 2022; Iketani et al., 2023; Moghadasi et al., 2023). Thus, intensive research has been carried out to find efficient therapies for the treatment and prevention of the current and future coronavirus outbreaks.

SARS-CoV-2, the pathogenic agent of the COVID-19 outbreak, is a positive-strand RNA virus belonging to the genus betacoronavirus, whose members also include the Middle East Respiratory Syndrome Coronavirus (MERS-CoV) and Severe Acute Respiratory Syndrome Coronavirus (SARS-CoV) (Aggarwal et al., 2021). Its genome encodes four structural proteins, and a series of 16 nonstructural proteins (NSP1-NSP16) that play important roles in RNA synthesis and processing, contributing to coronavirus survival and virulence power (Yadav et al., 2021; Biswas et al., 2021). Among these, NSP12 is one of the most important proteins required for viral growth, being the core component of the replication and transcription machinery of SARS-CoV-2 through its RNA-dependent RNA polymerase (RdRp) activity (Narayanan et al., 2022; Biswal et al., 2021).
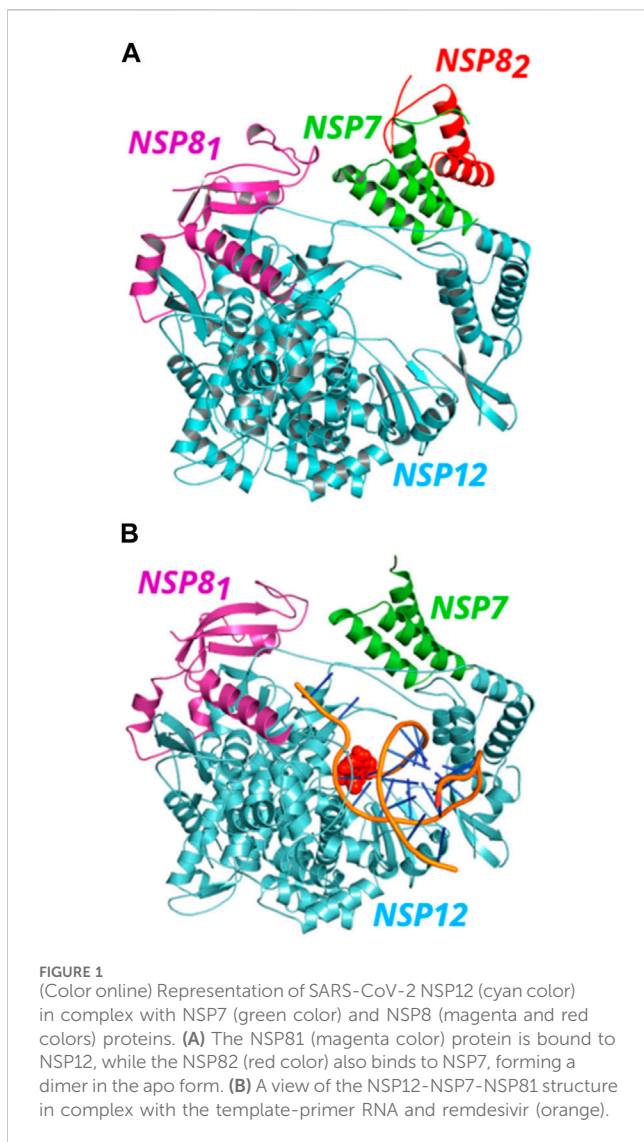
Due to its key role in the viral cycle, several papers have been published aiming to provide alternatives for inhibiting NSP12 function (Elkarhat et al., 2022; Bagabir, 2023; Giannetti et al., 2023; Gu et al., 2023). However, up to now, the FDA only approved the antivirals Molnupiravir and remdesivir targeting NSP12, both acting in different ways, with the last being covalently incorporated into the primer strand of replicating viral RNA, terminating chain elongation (Kabinger et al., 2021). However, the effectiveness of both drugs is disputed (Consortium et al., 2021; Butler et al., 2023), and the development of new drugs that can impair or, at least, reduce the functioning of the RdRp could be helpful.

It has been shown that NSP12 exhibits weak catalytic activity by itself in coronavirus, needing support from NSP7 and NSP8 cofactors to increase its binding to the template-primer RNA and enhance the polymerase activity (Peng et al., 2020; Kirchdoerfer and Ward, 2019). Structural analysis of the NSP12-NSP7-NSP8 super complex showed that it is stable as a 1:1:2 complex, with 2 NSP8 proteins ($NSP8_1$ and $NSP8_2$), and 1 NSP7 bound to NSP12. The precise role of NSP7 is still unclear, but, because of its affinity for NSP8 and lack of affinity for RNA, it has been suggested that its role may be to off-load RNA from NSP8 (Gu et al., 2023). On the other hand, it has been shown that mutations in NSP8 have also been associated with the altered synthesis in SARS-CoV-2 (Anjum et al., 2022; Reshamwala et al., 2021) observed that the mutations in NSP7 and NSP8 proteins are significantly associated with mutations NSP12, as a possible compensatory effect to maintain its function. Besides, the amino acid sequence of the three proteins and the binding site for the dimer NSP7-NSP8 in NSP12 are conserved across the coronavirus family (Kirchdoerfer and Ward, 2019), while mutations of some interface residues lead to weakened RNA replication activity of the RdRp machinery (Biswal et al., 2021).

In this sense, the impairment of the interaction between the proteins that form the NSP12-NSP7-NSP8 super complex could be a quite useful strategy to have some control over the SARS-CoV-2 infection, and the level of conservation of these proteins within the coronavirus family makes it a potential target not only for the current pandemic but also to future outbreaks. Thus, computational and experimental studies have been proposed to evaluate the interactions among these proteins, looking to understand and impair them (Ruan et al., 2021; Mutlu et al., 2022; Sarma et al., 2022). However, the authors are not aware of another study seeking to evaluate and rank the most relevant residue-residue interactions at a quantum level of theory, as well as investigate if the introduction of the viral RNA plus the remdesivir drug can alter the interaction pattern between these proteins since the active site of the NSP12 polymerase is very close to the NSP12-NSP7-NSP8 binding interface.

Protein-protein interactions (PPIs) play an essential role in regulating biological processes. Therefore, investigating these interactions is a crucial step for targeting the interfaces between proteins and using them in drug discovery (Cukuroglu et al., 2014). Understanding the PPI sites is essential to finding hotspots, i.e., certain residues or regions of the proteins that contribute more to the binding energy than other areas (Scott et al., 2016). Therefore, the efforts of many research groups are aimed at both the identification and the search for ways to modulate these hotspots (Ershov et al., 2022). Among the most commonly used computational methods to study the PPIs, are those based on classical molecular dynamics, alanine-scanning, hybrid quantum mechanics/molecular mechanics (QM/MM), and fully Quantum Mechanics (QM) methods (de Oliveira et al., 2020). The latter is becoming popular for this purpose because it provides a good description of the molecular geometries, (relative) binding affinities, and electronic states in the system with high accuracy.

FIGURE 1
(Color online) Representation of SARS-CoV-2 NSP12 (cyan color) in complex with NSP7 (green color) and NSP8 (magenta and red colors) proteins. **(A)** The NSP81 (magenta color) protein is bound to NSP12, while the NSP82 (red color) also binds to NSP7, forming a dimer in the apo form. **(B)** A view of the NSP12-NSP7-NSP81 structure in complex with the template-primer RNA and remdesivir (orange).

This is mainly due to its natural advantage of modeling polarization and charge transfer explicitly, becoming a suitable tool in all phases of *in silico* drug design (Zhou et al., 2010; Raha et al., 2007).

Unfortunately, the large number of atoms in biological molecules makes the accurate complete quantum mechanical description of the interaction energies for proteins with their ligands very costly, especially considering the interaction between proteins. In the last years, linear scaling approaches have been developed to make biological molecules computationally less expensive (Merz, 2014). The fragment-based ones represent an important class, with several schemes of protein decomposition applied to obtain protein properties, including the molecular fractionation with conjugate caps (MFCC), fragment molecular orbital (FMO), molecular tailoring approach (MTA), and generalized energy-based fragmentation (GEBF) (Ryde and Söderhjelm, 2016). Among these schemes, MFCC has been widely employed to calculate the interaction energy between protein amino acids and ligands, as well as in protein–protein complexes, allowing the investigation of a large number of amino acid residues in a protein possible with a small computational cost

and high accuracy (Lima Neto et al., 2015; Lima Neto et al., 2018; Bezerra et al., 2019; Albuquerque et al., 2021; Tavares et al., 2021). Recently, the MFCC scheme was used to study the interaction between the hACE-2 and Spike proteins of SARS-CoV-1, SARS-CoV-2, and hCoV-NL63 (Lima Neto et al., 2022), the SARS-CoV-2 Mpro with synthetic peptides (Amaral et al., 2022), and the human leukocyte antigen (HLA-A2) in complex with tumor-associated antigens based on glycoprotein gp100 (Pereira et al., 2021).

Therefore, this work aims to present a first detailed description of the interaction between NSP12-NSP7, NSP12-NSP8$_1$, and NSP12-NSP8$_2$ proteins at a quantum mechanical level of calculation. For this purpose, we have employed quantum biochemistry techniques within the density functional theory (DFT) framework and molecular fractionation with conjugate caps scheme to calculate the individual contribution of each amino-acid residue for the protein-protein interface. Besides, the complexes in the *apo* form and the presence of the template-primer RNA with remdesivir were used to search for structural and energetic differences between the interaction patterns, since the entrance of the RNA structure in NSP12 occurs close to the region in which it binds to NSP7 and NSP8.

2 Materials and methods

2.1 Protein-protein complex data and quantum calculations

The structural data of the SARS-CoV-2 RNA polymerase complex (NSP7, NSP8, and NSP12 proteins) solved in the *apo* form (PDB ID: 6M71; 2.90 Å of resolution) (Gao et al., 2020), and with a 50-base template-primer RNA and remdesivir (PDB ID: 7BV2; 2.50 Å of resolution) (Yin et al., 2020), based on a high-resolution description of expertly validated and curated structures in the crystal environment (Burley et al., 2019), not taking into account any dynamics process. We are aware that considering multiple structures could significantly improve the description of protein-ligand and protein-protein interactions, as shown in Ref (Liu et al., 2015). Nevertheless, the sampling of alternative refinement models through MD simulations may bring about a higher computational cost, particularly for large protein targets. Although higher computational cost is certainly not a reason to expect that computed effects are less relevant, the qualitative behavior of individual interaction energies cannot change considerably, i.e., the most energetically relevant residues could be similar by taking into account single or multiple structures.

It is important to mention that, in the *apo* form, the RNA polymerase structure from the PDB ID: 6M71 showed one NSP12 protein, one NSP7, and two NSP8 (here termed NSP8$_1$ and NSP8$_2$), while in the PDB ID: 7BV2, only one structure of each protein is found. See Figures 1A, B to observe the position of each protein in the complexes. NSP12 protein is colored in cyan, while NSP7, NSP8$_1$, and NSP8$_2$ proteins are represented in green, magenta, and red, respectively. The position of NSP8$_1$ and NSP8$_2$ in the complex follows the reference (Gao et al., 2020). In this work, we only took into account the residues present in the crystal structures and some missing residues may have an important impact on the results, mainly the residues at the beginning and end of the

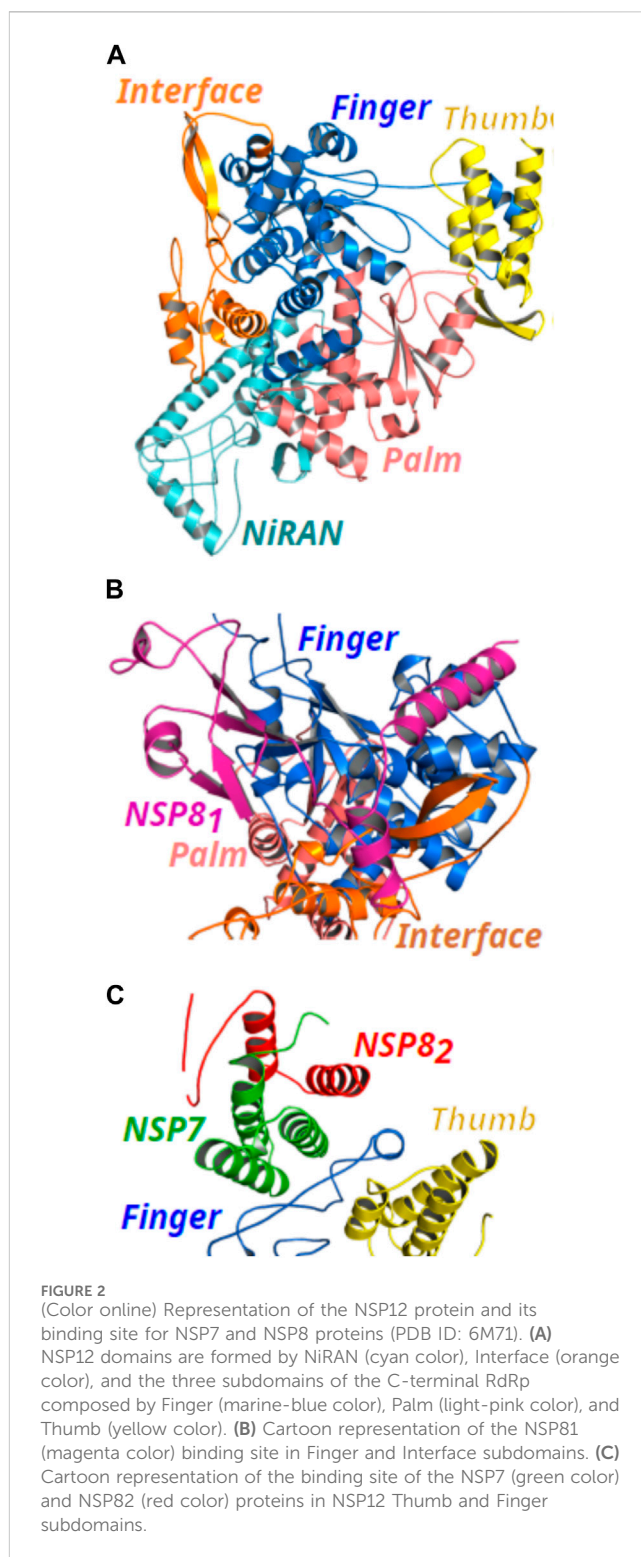NSP7 and NSP8 proteins, that could be in close contact with NSP12 and interact with some of its residues.

We added missing heavy atoms in the proteins, submitted the complexes to the PROPKA 3.1 package (Søndergaard et al., 2011), and included hydrogen atoms in the proteins according to the protonation study, as well as added the hydrogen atoms for the water molecules present in the crystal 7BV2. Afterward, protein main-chain heavy atoms are constrained, and the other atoms are submitted to a classical energy minimization using the Chemistry at Harvard Molecular Mechanics (CHARMm) force field (Momany and Rone, 1992), with the convergence tolerances to 10^{-5} kcal mol^{-1} (total energy variation) and 10^{-2} kcal mol^{-1}Å^{-1} (RMS gradient). Since the PROPKA software is slightly sensitive to the ligand pocket geometry, the steps of hydrogen addition/withdrawal and energy minimization are carried out until no difference is observed in the protonation results (Lima Neto et al., 2019).

After the energy minimization step, the dimers NSP12-NSP7, NSP12-NSP8$_1$, and NSP12-NSP8$_2$ (when they exist) were fragmented following the MFCC scheme (Zhang and Zhang, 2003; da Costa et al., 2012) (see below). The structures generated were submitted to energetic quantum mechanical calculations through the Gaussian (G16) package (Frisch, 2016). The generalized gradient approximation (DFT-GGA) functional B97D (da Costa et al., 2012) was selected to perform the quantum *in silico* simulation with the 6-311+G(d,p) basis set. This functional belongs to one of the most accurate general-purpose GGAs, reaching, for example, for the G97/2 set of the heat of formations, a mean absolute deviation of only 3.8 kcal mol^{-1}. The performance for noncovalently bound systems including many pure van der Waals complexes is excellent, reaching the average CCSD(T) accuracy (Grimme, 2006). Moreover, it improves the accuracy of describing the atom's electronic structure and consequently, the molecular interactions and (relative) binding affinities, which are pivotal to macromolecular systems in the context of drug lead discovery and design (De Sousa et al., 2017; Bezerra et al., 2020; Vianna et al., 2021; Santos et al., 2022).

The effect of the residues surrounding formed by neighboring atoms (amino acids and water molecules) was included in our calculations using the conductor-like polarizable continuum model (CPCM) (Barone and Cossi, 1998; Cossi et al., 2003) through the dielectric constant ε_{40}, which represents well the influence of electrostatic environment surrounding the residue-residue complex (Vicatos et al., 2009; Tavares et al., 2018; Campos et al., 2020; Morais et al., 2020).

2.2 Molecular fractionation with conjugate caps

As presented above, we fragmented the proteins into amino acids following the MFCC scheme, as in reference (Rodrigues et al., 2013). In the framework of this approach, for each amino acid of interest of the NSP12 at position R_i, we mapped its distance to the residues in the proteins NSP7, NSP8$_1$, and NSP8$_2$ at position R_j and chose those R_i–R_j pairs, that showed at least one atom inside a radius (r) equal to 8.0 Å. Thus, R_i and R_j were decomposed into individual fragments by cutting through the peptide bonds and a pair of conjugate caps was designed to saturate each fragment,

FIGURE 2
(Color online) Representation of the NSP12 protein and its binding site for NSP7 and NSP8 proteins (PDB ID: 6M71). **(A)** NSP12 domains are formed by NiRAN (cyan color), Interface (orange color), and the three subdomains of the C-terminal RdRp composed by Finger (marine-blue color), Palm (light-pink color), and Thumb (yellow color). **(B)** Cartoon representation of the NSP81 (magenta color) binding site in Finger and Interface subdomains. **(C)** Cartoon representation of the binding site of the NSP7 (green color) and NSP82 (red color) proteins in NSP12 Thumb and Finger subdomains.

aiming to preserve the local chemical environment and comply with the valence requirements. Here, the caps are formed by the neighbor residue covalently bound to the amine (C_i and C_j) and carboxyl (C_{i^*} and C_{j^*}) groups of residues R_i and R_j, respectively, along the protein chain. This provides a better description of its electronic environment. Hydrogen atoms are added to the molecular caps to avoid dangling bonds (He et al., 2014). Finally, the interaction

energy (IE) of each residue-residue pair, IE(R_i–R_j), was calculated as follows in Equation 1:

$$IE(R_i - R_j) = E(\Delta_{ij}) - E(\Delta_i \delta_j) - E(\delta_i \Delta_j) + E(\delta_{ij}),$$

where $\Delta_m = C_m R_m C_{m^*}$ and $\delta_m = C_m C_{m^*}$ ($m = i, j$). The term $E(\Delta_{ij})$ corresponds to the total energy of the fragment comprised of both capped residues. The second and the third terms of the equation, $E(\Delta_i \delta_j)$ and $E(\delta_i \Delta_j)$, give the total energy of the system formed by the capped residue R_i and R_j and the hydrogenated caps of R_j and R_i, respectively. $E(\delta_{ij})$ is the total energy of the system formed only by the caps. Additionally, to achieve the structural stability of the complex promoted by interactions with the extended hydration network, all water molecules forming hydrogen bonds with a particular residue or cap were included for completeness in the fragments. The descriptions of the interaction types were obtained through the Discovery Studio visualizer (Biovia Dassault Systèmes, 2021) and visual inspection.

3 Results and discussion

In this work, quantum mechanical calculations were employed to describe residue-residue interactions and highlight the hotspots on the protein's surface. This is a valuable strategy in drug design because it allows the identification of druggable sites. For the completeness of the analysis, not only residues located at the interface but all residues within 8.0 Å from the interface of the proteins were analyzed (Silva et al., 2020; Lima Neto et al., 2022). A schematic representation of the proteins is shown in Figure 2. The structure of the NSP12 (Figure 2A) is formed by two domains connected by an Interface domain (residues 250-365; orange): an N-terminal nidovirus RdRp-associated nucleotidyltransferase (NiRAN) domain (residues D60-R249; cyan), and a C-terminal right-handed RdRp domain (residues 366-920). The C-terminal RdRp is also divided into three subdomains: Finger (residues 366-580 and 620-678; marine-blue), Palm (residues 581-619 and 679-814; light-pink), and Thumb (residues 815-932; yellow), which is a conserved architecture in all viral RdRps (Padhi et al., 2021; Tian et al., 2021).

In Figures 2B, C, we present the binding site for NSP8$_1$, NSP7, and NSP8$_2$, respectively. As one can see, NSP8$_1$ clamps the top region of the Finger subdomain (marine-blue color) and also forms additional interactions with the Interface domain (orange color). On the other hand, the NSP7-NSP8$_2$ dimer binds above the Thumb subdomain (yellow color) of NSP12 and sandwiches the Finger loops, possibly to stabilize its conformation with NSP7 mediating most of the interactions in the dimer with NSP12, whereas, only a small region of NSP8$_2$ looks to be in close contact with NSP12 residues.

Evaluating our results, we observed that in the supercomplex NSP12-NSP7-NSP8 solved in the *apo* form (PDB ID: 6M71), a total of 48 residues of NSP12, and 44 residues belonging to NSP7 were considered in the analysis of the PPIs in the dimer NSP12-NSP7. Furthermore, 122 residues of NSP12 and 88 residues of NSP8$_1$ were analyzed in the dimer NSP12-NSP8$_1$, resulting in 313 residue-residue interaction

pairs with the energy calculated for the first dimer (NSP12-NSP7) and 866 for the second one (NSP12-NSP8$_1$). The last PPIs studied in this PDB structure were in the NSP12-NSP8$_2$ dimer, where NSP8$_2$ contributed with 9 residues and NSP12 with 16, totalizing 38 interaction pairs. In the super complex NSP12-NSP7-NSP8 solved with the template-primer RNA and redeliver (PDB ID: 7BV2), 43 (87) residues of NSP7 (NSP8$_1$), and 51 (126) residues of NSP12 (NSP8$_1$) were considered in the analysis of the PPIs in NSP12-NSP7 (NSP12-NSP8$_1$), resulting in 326 (849) residue-residue interaction pairs with energy calculated.

To facilitate the identification when we are referring to the analysis of the PPIs in the proteins of the PDB 6M71 or the 7BV2 crystals, we included the superscript APO and RNA in protein/residue names, respectively. The total interaction energy (TIE) of the dimers was calculated as the sum of pairwise interactions in each complex: NSP12-NSP7^{APO} (−90.24 kcal mol^{-1}), NSP12-NSP7^{RNA} (−85.28 kcal mol^{-1}), NSP12-NSP8$_1$^{APO} (−320.93 kcal mol^{-1}), NSP12-NSP8$_1$^{RNA} (−327.58 kcal mol^{-1}), and NSP12-NSP8$_2$^{APO} (−19.44 kcal mol^{-1}).

Unfortunately, as we know, there is no experimental data to compare with these energy outcomes. However, (Sarma et al., 2022), calculated the binding free energy (BFE) of the two dimers, NSP12-NSP7 and NSP12-NSP8 (PDB ID: 6M71), through molecular dynamics simulation and the MM/PBSA scheme, showing that the second dimer has a stronger binding energy than NSP12-NSP7, as we observed for both structures here studied. (Wilamowski et al., 2021) observed that the NSP12-NSP7-NSP8 super complex is more stable after the binding of the RNA molecule, but they suggested that NSP7 and NSP8 are static components, helping to close the complex once RNA is bound, guiding the RNA upon exit, and stabilizing contacts with other proteins in the replication/transcription process. Our energetic results were quite close between the *apo* form, and that bound to the RNA+remdesivir. Hence, further studies are necessary to understand the stability of the supercomplex in the presence/absence of RNA, as well as with RNA plus the inhibitor remdesivir.

It is worth mentioning that the central idea of this work is not to supply the complete binding mechanism but to describe the intermolecular interaction energies between NSP12-NSP7/NSP8, identifying the most important interactions present in the crystallographic structures. Thus, our computational results correspond to a view of the static molecular momentum of these proteins. It is important to mention that beyond the interaction energy (enthalpic effect) here obtained, protein-protein binding is also governed by other factors, including (de)hydration, hydrophobic effects, and entropic contributions, and the interaction between residues of the same protein (intramolecular) that could also help in the stabilization of a certain structural conformation, not considered in this work. These can induce changes in the solvent interaction interface and the formation or breaking of intermolecular interactions.

Taking into account the dynamic nature of the biomolecules, a classical molecular dynamics (MD) approach, with adequate phase space sampling, might provide a more realistic dynamic structure. However, unfortunately, it gives poor accuracy in describing the interaction energies depicted in this work, as compared to a

TABLE 1 Energy values (in kcal mol^{-1}) of the most energetically relevant residue-residue interaction pairs for the dimer NSP12-NSP7.

NSP12–NSP7 residues	Energy (kcal mol^{-1})	
	NSP12-NSP7^{APO}	NSP12-NSP7^{RNA}
K411–Q18	−2.57	−1.71
K411–E23	−2.57	−1.23
F415–C8	**−3.78**	−3.10
Y420–S4	−2.76	−1.62
F429–S4	−2.04	−1.91
E431–K2	−2.32	**−3.63**
F440–K7	−1.85	−2.15
F440–L40	−1.81	**−3.24**
F442–L40	−1.97	−2.15
F442–L41	−1.19	−2.07
A443–N37	**−4.28**	**2.46**
Q444–W29	−1.66	−2.08
D445–V33	−2.09	−1.39

The strongest attractive (repulsive) interaction energies are shown in bold red (bold blue).

quantum chemistry approach (Ryde and Söderhjelm, 2016). Therefore, we have used molecular quantum chemistry calculations based on the DFT scheme, which is a route to investigate accurately large biological systems with affordable computational cost. It has been successfully employed previously to describe ligand-protein interactions at the quantum level (for a review see the recent book (Albuquerque et al., 2021), and the references therein).

One of the most significant properties of the PPI interface is that the energy is not uniformly distributed, and the hotspot residues have the greatest impact on binding energy in the protein complex (Bogan and Thorn, 1998). To evaluate the hotspot residues across the PPI interfaces in the dimers NSP12-NSP7 and NSP12-NSP8, we calculated all the residue-residue interaction energy (IE) within a r equal to 8.0 Å and presented the most energetically significant ones below. Here, the results are presented and discussed following the order NSP12-NSP7, NSP12-NSP8$_1$, and NSP12-NSP8$_2$. When the dimer is present in both crystal structures, they are also compared in the same subsection.

3.1 Analysis of the NSP12−NSP7 dimer interactions

Table 1 depicts the 13 interaction pairs showing an energy value stronger than 2.0 or −2.0 kcal mol^{-1} at least in one of the two complexes studied. From these, 8 interaction pairs were within the energy cutoff in the complex NSP12-NSP7^{APO}, with the strongest interaction energies (IEs) found in the pairs A443-N37^{APO}, and F415-C8^{APO}, while the weakest IEs were found in the pairs F429-S4^{APO}, and E445-V33^{APO}. In the dimer NSP12-NSP7^{RNA}, the strongest IEs were observed in the pairs E431-K2^{RNA}, and F440-

L40^{RNA}, while the weakest interaction energies were observed in the pairs F442-L41^{RNA}, and Q444-W29^{RNA}. The residue-residue pairs showing the strongest interaction energies have the IE highlighted in bold red, whereas those showing the weakest IEs were in bold. Besides, the IE of the pair A443-N37^{RNA} is in bold blue because it is the only residue-residue pair presenting positive (repulsion) interaction energy among the 13 selected.

As one can see, by comparing NSP12-NSP7^{APO} with NSP12-NSP7^{RNA}, most of the IEs are quite close, indicating a similar interaction pattern, and that only small shifts occurred in the protein after the introduction of the RNA+remdesivir to the complex. In Figure 3, we depict the most energetically relevant interaction pairs of NSP12-NSP7^{APO} (left) and NSP12-NSP7^{RNA} (right). Three types of intermolecular interactions dominate the residue-residue pairs: hydrogen bonds (H-bonds), non-conventional H-bonds, and π-alkyl, albeit an electrostatic (ion-ion) interaction and a repulsion were also observed. We present these interactions below, followed by a comparison between the two complexes studied.

A443-N37^{APO} is the residue-residue pair showing the strongest interaction energy among those analyzed from both complexes. The polar atoms of the alanine main chain make two H-bonds with the two polar atoms of the asparagine's side chain at 2.1 and 2.7 Å (Figure 3A). On the other hand, the pair A443-N37^{RNA} is the only one presenting a positive (repulsive) IE. Looking at Figure 3B, one can see that the side chain of N37 rotates (see Supplementary Figure S1A), so its group NH^2 is close to the main chain NH of N443 (1.8 Å) forming a repulsion between the residues, whereas an H-bond is also formed (2.6 Å). In Supplementary Figure S2, we present the electrostatic potential map showing the region in blue depicting the repulsion between the NH groups (blue), as well as between the oxygen atoms (red) of the residues. According to (Biswal et al., 2021), the mutation of N37 to valine (N37V) greatly
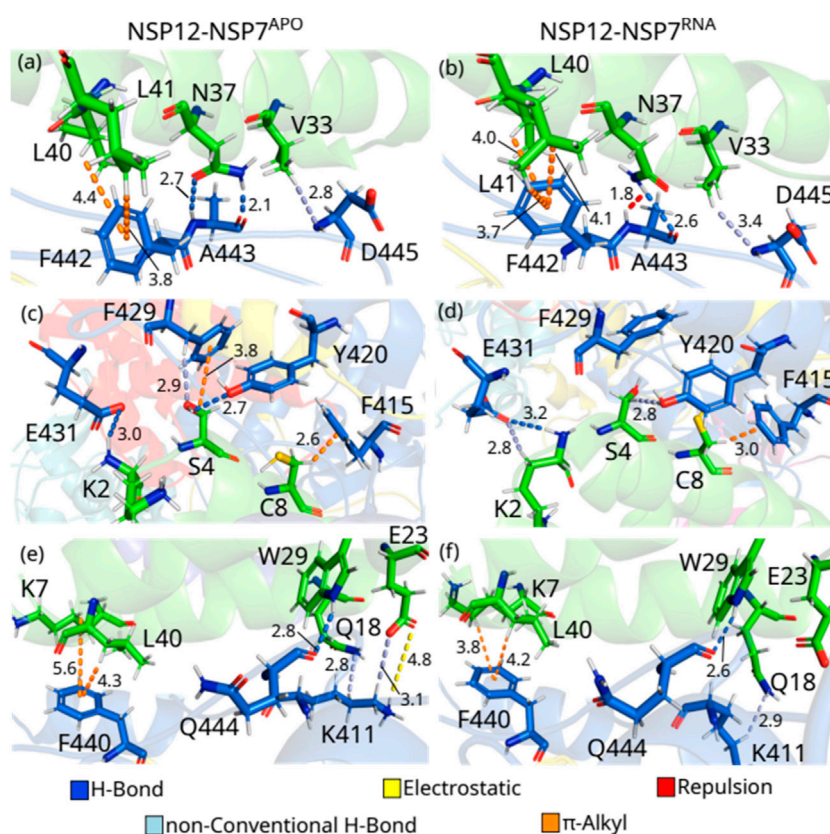
FIGURE 3
(Color online) Detailed spatial arrangement of the major NSP12-NSP7 interaction pairs with their intermolecular interaction in PDB ID 6M71 [left - **(A)**, **(C)** and **(E)**] and 7BV2 [right **(B)**, **(D)** and **(F)**]. Dashed lines in marine (light-blue) represent direct (non-conventional) hydrogen bonds, while orange (yellow) lines represent π-alkyl (electrostatic) interactions. Repulsion is represented by red lines.

hampers RdRp activity of SARS-CoV-2 NSP12-NSP7-NSP8 since it disrupts the hydrogen bond formed with A443, but the stability of NSP7–NSP8 is maintained. (Subissi et al., 2014) performed a mutation in N37 (to alanine) of SARS-CoV, observing that it impairs the RdRp activity of the protein, which reinforces the conservation of the binding site of NSP12-NSP7 among different CoVs. Noteworthy (Sarma et al., 2022), evaluated the binding of these proteins through molecular dynamics simulation together with MM/PBSA analysis, finding that N37 plays an important role in the formation of NSP12-NSP7 complex in SARS-CoV-2 through the formation of H-bonds, although its role in SARS-CoV was not completely elucidated.

D445-V33^{APO} presents one of the weakest IE within our energy cutoff, and the interaction energy of D445-V33^{RNA} is still weaker. In both cases, the residues are making a non-conventional H-bond between the main chain of D445 and the side chain of V33, but at different distances, with the first at 2.8 Å and the second at 3.4 Å (Figures 3A, B). In the pairs, F442-L40 and F442-L41 occur the opposite of what has been observed so far, with the NSP12-NSP7^{APO} pair showing a weaker IE than the NSP12-NSP7^{RNA} one. F442-L40^{APO} forms a π-alkyl interaction with a distance of 4.4 Å, while the same interaction is found in F442-L40^{RNA}, but at a shorter distance (4.0 Å). Similarly, the pair F442-L41^{APO} also makes a π-alkyl interaction (3.8 Å), and there is a reorganization in the side chain of F442, as well as in L41 in the crystal with RNA (see Supplementary

Figure S1A) that allows the formation of a second π-alkyl interaction (3.7 and 4.1 Å). As we know, the relevance of these residues was not previously reported.

F415-C8^{APO} shows one of the strongest IE, and it is quite close to the interaction energy found in the pair F415-C8^{RNA}. In both cases, these residues are making a π-alkyl interaction at the distance of 2.6 Å (Figure 3C) and 3.0 Å (Figure 3D), respectively, besides some other hydrophobic contacts. It was previously shown that the mutation of the residue C8 to glycine (C8G) leads to a severe reduction of RdRP efficiency since it interacts with residues at the interface of NSP8 and NSP12 (Biswal et al., 2021), as well as (Sarma et al., 2022) observed the relevance of this residue not only for SARS-CoV-2 but also to SARS-CoV.

S4^{APO} interacts with Y420^{APO} and F429^{APO} and presents IE within our energy criteria. As one can see in Figure 3C, S4^{APO} is forming an H-bond with Y420^{APO} (Y420-S4^{APO}: 2.7 Å), while a π-alkyl (3.8 Å) interaction and a non-conventional H-bond (2.9 Å) are made with F429^{APO}. On the other hand, there is a rotation in the side chain of S4^{RNA} (see Supplementary Figure S1B) that impairs the formation of the same intermolecular interactions. Thus, Y420-S4^{RNA} is making a non-conventional H-bond (2.8 Å), while only small hydrophobic contacts were observed in the pair F429-S4^{RNA}. Despite the residue serine 4 being part of the interface interacting with NSP8 and NSP12, we do not find any other study showing the role of this residue in the
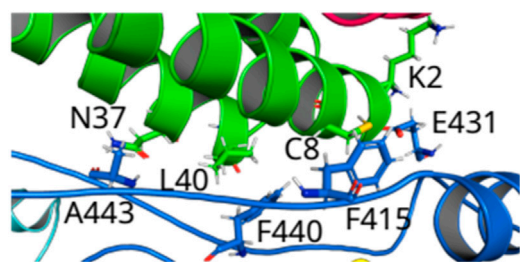
FIGURE 4
(Color online) Overview of the loops connecting Finger-Thumb regions from NSP12 to the helices of NSP7. Hotspot regions in NSP12--NSP7 formed by the amino acids that make hydrogen bonds (E431--K2 and A443--N37) and -alkyl interactions (F415--C8 and F440—L40).

activity of SARS-CoV-2 NSP12-NSP7-NSP8 supercomplex, although the Ref. (Sarma et al., 2022) also showed Y420 and F429 as important residues to the interface.

E431-K2^{RNA} is the strongest interaction energy among the residue-residue pairs studied in the NSP12-NSP7^{RNA} dimer, and the third by comparing all the pairs in this section, whereas E431-K2^{APO} shows the fifth-strongest IE of NSP12-NSP7^{APO}. As one can see in Supplementary Figure S1B, these residues are rearranged in E431-K2^{RNA}, which leads to the formation of not only one H-bond (3.2 Å; Figure 3D), as in E431-K2^{APO}

(3.0 Å; Figure 3C), but also a non-conventional H-bond (2.8 Å; Figure 3D), increasing the interaction energy of the pair. K411^{APO} interacts with Q18^{APO} and E23^{APO}, making a non-conventional H-bond with both of them at a distance of 2.8 Å and 3.1 Å (Figure 3E), respectively, while it also forms an electrostatic interaction with E23^{APO} (4.8 Å) and some hydrophobic interactions with Q18^{APO}. However, the position of the side chain of K411^{RNA} shifts and moves away from E23^{RNA} in NSP12-NSP7^{RNA} and no direct interaction was observed, while the non-conventional H-bond with Q18^{RNA} is maintained (2.9 Å; Figure 3F).
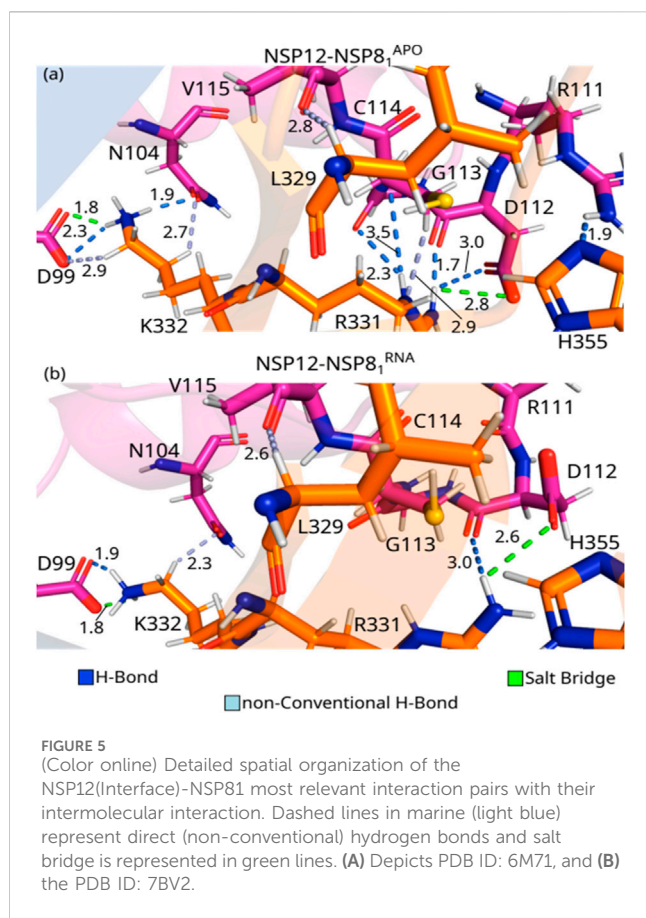
Q444-W29 are forming H-bonds at 2.8 and 2.6 Å in NSP12-NSP7^{APO} and NSP12-NSP7^{RNA}, respectively (Figures 3E, F). F440 interacts with K7 and L40 through a π-alkyl interaction in both complexes here analyzed (Figures 3E, F). Interestingly, in both cases, the IEs observed in these pairs are stronger in NSP12-NSP7^{RNA} than NSP12-NSP7^{APO} with interaction distances shorter in the first one. The key role of F440, K7, and L40 for the binding energy of the complex was shown by (Sarma et al., 2022), while the residue K7 of SARS-CoV (NSP7) is found to be essential for RdRp activity (Subissi et al., 2014). Thus, we observed that the two loops that connect the Finger-Thumb regions of NSP12 and the top of the helices that form NSP7 are very relevant to the interaction between these to protein (see Figure 4), as well as break the H-bonds in the pairs E431-K2 and A443-N37, and the π-alkyl interactions in the pairs F415-C8 and F440-L40 could be important to impair the RdRp activity of the complex.

TABLE 2 Energy values (in kcal mol^{-1}) of the most important residue-residue interaction pairs for the dimer NSP12-NSP8.

NSP12−NSP8$_1$	Energy (kcal mol^{-1})	
Residues	NSP12-NSP8$_1$^{APO}	NSP12-NSP8$_1$^{RNA}
L514–K79	−3.43	−4.71
D517–K79	−4.42	−4.38
D523–R80	−1.22	−5.36
S384–M94	**5.33**	−2.48
S384–K97	−3.51	−5.71
G385–K97	−4.12	−2.60
K332–D99	**−14.74**	**−11.63**
K332–N104	−6.45	−2.22
H355–R111	−5.77	−0.16
R331–D112	**−8.16**	−4.66
R331–G113	−4.80	−0.65
R331–C114	−4.72	0.49
L329–V115	−4.40	−4.76
N386–K127	−0.78	−5.45
L387–L128	−5.62	−6.45
L388–M129	−1.66	−5.71
L389–V130	−5.30	**−6.53**

The strongest attractive (repulsive) interaction energies are shown in bold red (bold blue).

FIGURE 5
(Color online) Detailed spatial organization of the NSP12(Interface)-NSP81 most relevant interaction pairs with their intermolecular interaction. Dashed lines in marine (light blue) represent direct (non-conventional) hydrogen bonds and salt bridge is represented in green lines. **(A)** Depicts PDB ID: 6M71, and **(B)** the PDB ID: 7BV2.

3.2 Analysis of the NSP12−NSP8₁ and NSP12−NSP8₂ interactions

By analyzing the individual interaction energy of the residue-residue pairs in the dimer NSP12-NSP8[1], we observed that more than 50 pairs showed IE over the energy criteria used in the last subsection, i.e., stronger than 2.0 or −2.0 kcal mol⁻¹ at least in one of the two complexes studied (see Supplementary Table S1). Therefore, we increased the IE cutoff to values stronger than 4.0 or −4.0 kcal mol⁻¹ to present only the most relevant interactions to the complex. Hence, 17 residue-residue pairs were selected and are shown in Table 2. From these, 14 interaction pairs were within the energy cutoff in the complex NSP12-NSP8$_1^{APO}$, with the strongest interaction energies (IEs) found in the pairs K332-D99^{APO}, and R331-D112^{APO}, while the weakest IEs were found in the pairs S384-K97^{APO}, and L514-K79^{APO}. In the dimer NSP12-NSP8$_1^{APO}$, the strongest IEs were observed in the pairs K332-D99^{RNA}, and L389-V130^{RNA}, while the weakest interaction energies were observed in the pairs R331-D112^{RNA}, and D517-K79^{RNA}. The residue-residue pairs showing the strongest interaction energies have the IE highlighted in bold red, whereas those showing the weakest IEs were in bold. Besides, the pair S384-M94^{APO} is in bold blue because it is the only residue-residue pair presenting positive (repulsion) interaction energy among the 17 selected.

As one can see, contrary to what was previously observed in the NSP12-NSP7 dimer, the difference between most of the IEs (11) in

NSP12-NSP8$_1^{APO}$ and NSP12-NSP8$_1^{RNA}$ are > 2.0 kcal mol⁻¹, indicating that changes might have occurred in the interaction's pattern after the introduction of the RNA+remdesivir to the complex. Besides, two regions of NSP12 (Interface and Finger) interact with NSP8₁ protein with IEs within our energy cutoff value. In Figure 5, we show the interaction pairs between the NSP12 (Interface) and NSP8₁: K332-D99, K332-N104, H355-R111, R331-D112, R331-G113, R331-C114, and L329-V115.

K332-D99^{APO} is the residue-residue pair showing the strongest IE among the three complexes studied in this paper. As one can see in Figure 5A, these residues are making a salt bridge (1.8 Å), as well as an H-bond (2.3 Å), and a non-conventional H-bond (2.9 Å). On the other hand, the pair K332-D99^{RNA} shows the second-strongest IE, forming a salt bridge (1.8 Å), and an H-bond (1.9 Å), see Figure 5B. K332^{APO} also interacts with N104^{APO} through an H-bond (1.9 Å) and a non-conventional H-bond (2.7 Å; Figure 5A), whereas K332-RN104^{RNA} only forms non-conventional H-bond (2.3 Å; Figure 5B). As shown in Supplementary Figure S1C, the shift in the side-chain of the lysine residue hindered the formation of the non-conventional H-bond in the K332-D99^{RNA} pair, as well as the H-bond with N104^{RNA}, which decreased its interaction energy, when compared to the crystal in the *apo* form. The per-residue energy contribution of N104, D99, and K332 was previously observed by Sarma et al. (2022) for SARS-CoV and SARS-CoV-2. The mutation D99A was observed to generate crippled *in vivo* phenotypes of SARS-CoV, with reduced plaque size and lower progeny titers (Subissi et al., 2014), that is because it disrupts the electrostatic interaction with K332 (Kirchdoerfer and Ward, 2019). Furthermore, no experimental study has shown the relevance of N104 yet.

R331-D112^{APO} presents one of the strongest IEs, and it is almost double the value of R331-D112^{RNA}. As one can see in Figure 5A, the side-chains of the pair R331-D112^{APO} are making two H-bonds (1.7 and 3.0 Å), and a salt bridge (2.8 Å), whereas the residues R331-D112^{RNA} are forming a salt bridge (2.6 Å), and an H-bond (3.0 Å; Figure 5B). R331^{APO} is also forming an H-bond with G113^{APO} (2.3 Å) and C114^{APO} (3.5 Å), a non-conventional H-bond (2.9 Å) and hydrophobic interactions with the residue C114^{APO}, see Figure 5A. Similar to what we observed in residue K332, the side-chain of R331 shifts, decreasing the number of interactions formed between the residues in the dimer with the presence of RNA (Supplementary Figure S1C). This shift in the side-chain of R331^{RNA} makes it impossible to form direct contact with G113^{RNA} and C114^{RNA}. Despite the strong interaction energy, the relevance of these residues was not tested experimentally, as the authors know, but (Sarma et al., 2022) obtained a high value of energy contribution for both residues in SARS-CoV-2.

L329-V115^{APO} and H355-R111^{APO} are among the pairs showing the strongest interaction energies. The IE between the residues L329-V115 is quite similar in both crystal structures, which corresponds to the formation of a non-conventional H-bond at the distance of 2.8 Å and 2.6 Å in NSP12-NSP8^{APO} and NSP12-NSP8$_1^{RNA}$, respectively. The residues in the pair H355-R111^{APO} are interacting by an H-bond (1.9 Å; Figure 5A). On the other hand, in the NSP12-NSP8$_1^{RNA}$ crystal, the shift in the side-chain position of R111 (Supplementary Figure S1C) makes H355-R111^{RNA} so far away that they no longer interact.
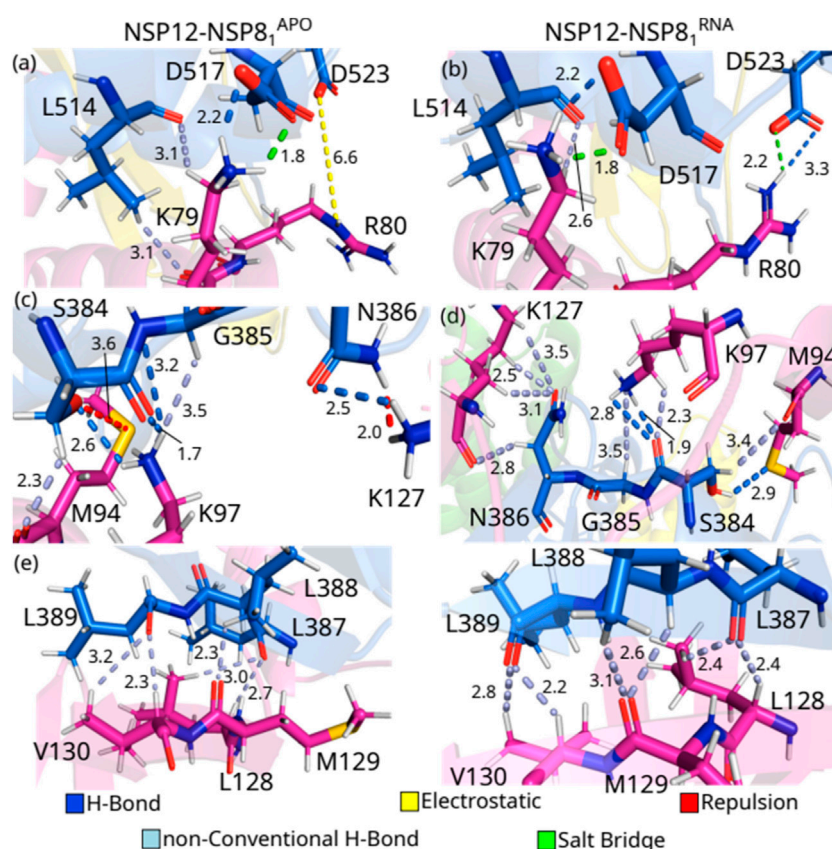
FIGURE 6
(Color online) Detailed spatial arrangement of the major NSP12(Finger)-NSP81 interaction pairs with their intermolecular interaction in PDB ID 6M71 [left - (A), (C) and (E)] and 7BV2 [right (B), (D) and (F)]. Dashed lines in marine (light-blue) represent direct (non-conventional) hydrogen bonds, while green (yellow) lines represent salt bridge (electrostatic) interactions. Repulsion is represented by red lines.

When the residues in the Interface region of NSP12 were taken into account, the calculated IEs were stronger for the crystal NSP12-NSP8$_1^{APO}$ compared to the NSP12-NSP8$_1^{RNA}$, while the opposite behavior can be observed in the interaction between the Finger region of the NSP12 protein and the NSP8$_1$ protein. In Figure 6, we depict the most relevant interaction pairs between the NSP12 (Finger) and NSP8$_1$: L514-K79, D517-K79, D523-R80, S384-M94, S384-K97, G385-K97, N386-K127, L387-L128, L388-M129, L389-V130.

One can see from Figure 6A that the residues L514-K79^{APO} form two non-conventional H-bonds at a distance of 3.1 Å each, and also hydrophobic interactions, while in the crystal with the RNA sequence, the hydrophobic interaction is maintained, but only one non-conventional hydrogen bond is observed, at a distance of 2.6 Å (Figure 6B). Residues D517 and K79 are making a salt bridge (1.8 Å) and an H-bond (2.2 Å) in both crystal structures. On the other hand, when we evaluated the interactions between the residues D523 and R80, we observed that the side-chain of D523-R80^{APO} is involved in electrostatic contacts, whereas a salt bridge (2.2 Å) and an H-bond (3.3 Å) are present in the crystal NSP12-NSP8$_1^{RNA}$.

S384 shows strong IEs when interacting with M94 and K97. Interestingly, S384-M94^{APO} presents the strongest positive (repulsion) energy, and it occurs even with the formation of

non-conventional H-bonds (2.3 Å). Looking at Figure 6C, one can observe that the oxygen atom from the serine side-chain and the sulfur atom from the methionine residue are very close to each other (3.6 Å), while in the NSP12-NSP8$_1^{RNA}$ crystal (Figure 6D), the hydroxyl group of the serine residue is making an H-bond (2.9 Å) with M94 besides the non-conventional H-bond (3.4 Å). By interacting with K97^{APO}, S384 makes two H-bonds (1.7 and 2.6 Å) with its side-chain NH$^+_3$ group, whereas it forms two H-bonds (1.9 and 2.8 Å) and a non-conventional H-bond (3.5 Å) with K97^{RNA} The residue K97 of NSP8$_1$ also interacts strongly with G385^{APO}, creating an H-bond (3.2 Å) and a non-conventional H-bond (3.5 Å). On the other hand, K97^{RNA} just makes a non-conventional H-bond (3.5 Å) with G385^{RNA}. Moreover, N386-K127^{APO} are forming an H-bond (2.5 Å) and repulsion between their NH side-chain groups (2.0 Å), and N386–K127^{RNA} are making 4 non-conventional H-bonds (2.5, 2.8, 3.1, and 3.5 Å).

Finally, the region formed by 3 leucines (L387, L388, and L389) in NSP12 shows the strongest interaction energies among the evaluated pairs of NSP12 (Finger)-NSP8$_1$. As one can see from Figures 6E, F, L387-L128 and L389-V130 are involved in two non-conventional H-bonds and hydrophobic interactions in both crystals, as well as L388-M129 form one non-conventional H-bond in NSP12-NSP8$_1^{APO}$ and two non-conventional H-bonds in NSP12-NSP8$_1^{RNA}$. Despite the energetic relevance
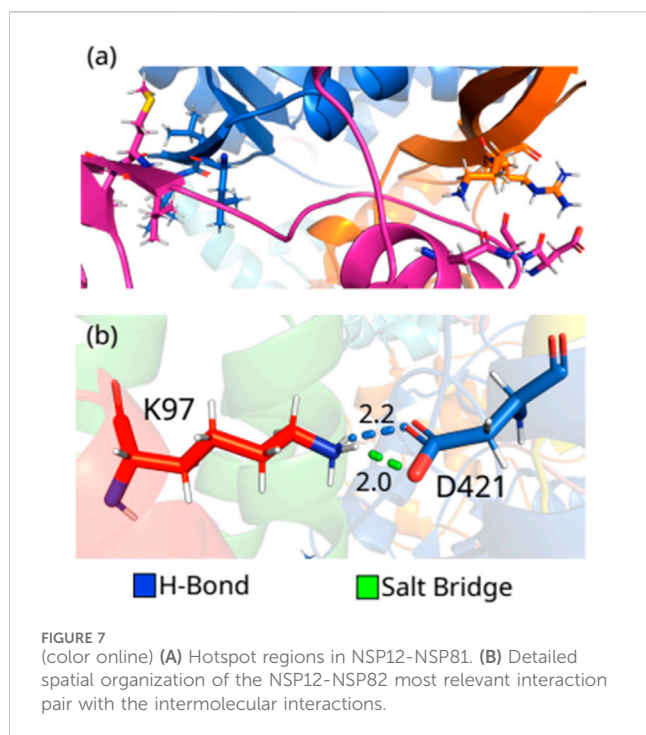
of the residues here presented, we could not find them in other
experimental or computational studies, except in the paper of
(Sarma et al., 2022). Hence, future works could be performed to
evaluate the role of these residues in the function of the complex.

Thus, we observed that the region of the protein in which two
positively charged residues (R331 and K332; Interface) are, forming
strong interactions (salt bridge and H-bond) with D99, N104, and
D112, could be a relevant target to break the interaction between
$NSP12$ and $NSP8_1$, as well as the region formed by the 3 leucine
residues (L387, L388, and L389; Finger) that are related to the
formation of several non-conventional H-bonds. These residues of
NSP12 interact with a region of $NSP8_1$ composed of the residues 99-
130, mainly the residues in the helix and the β-strand
(see Figure 7A).

In the end, we included the interaction between the proteins
in the dimer $NSP12$-$NSP8_2$ here because only one residue-
residue pair showed interaction energy stronger than 2.0 or
-2.0 kcal mol^{-1}. D421-K97 (-11.62) are making a salt bridge
(2.0 Å) and an H-bond (2.2 Å), as in Figure 7B, contributing
approximately 58% of the total interaction energy of the
complex. It is important to mention that the dimer
$NSP12$-$NSP8_2$ is only present in the crystal with ID: 6M71,
i.e., the $NSP12$-$NSP8_2{}^{APO}$. In Supplementary Tables S2, S3, we
resume the interactions made by the energetically most relevant
residue-residue pairs in NSP12-NSP7 and NSP12-NSP81,
respectively.

4 Conclusion

The indiscriminate spread of the coronavirus poses a threat to
human health around the world. NSP12 is the core component of
the replication and transcription machinery of SARS-CoV-2, and

the proteins NSP7 and NSP8 are essential for its function. This
suggests that compounds that could disrupt the binding of NSP7 or
NSP8 to the NSP12 complex might help to fight against the virus.
However, there are few residues at this complex's interface identified
as probable hotspots. We used quantum biochemistry methods to
investigate the interactions between the proteins in the dimers
$NSP12$-NSP7, $NSP12$-$NSP8_1$, and $NSP12$-$NSP8_2$, in atomic detail
to understand the process by which these proteins interact. We
aimed to discover hotspots that could be used to neutralize
viral infection.

According to the protein-protein interaction results, the total
interaction energy follows the order: $NSP12$-$NSP8_1$ > $NSP12$-
NSP7 > $NSP12$-$NSP8_2$. Evaluating the individual interaction
energies (IEs) between the residues, 14 pairs of $NSP12$-$NSP8_1$
presented the strongest IEs: L514-K79, D517-K79, S384-M94,
S384-K97, G385-K97, K332-D99, K332-N104, H355-R111, R331-
D112, R331-G113, R331-C114, L329-V115, L387-L128, and L389-
V130. In the complex NSP12-NSP7, we find 8 residue-residue pairs
with strongest IEs (K411-Q18, K411-E23, F415-C8, Y420-S4, F429-
S4, E431-K2, A443-N37, and D445-V33), whereas only one pair
(D421-K97) proved to be energetically relevant. Besides, we
observed that hydrophobic interactions are key for the dimer
NSP12-NSP7, while hydrogen bonds are the most relevant for
NSP12-NSP8. Unfortunately, as far as we know, there is no
experimental data to compare with our total interaction energy
outcomes. On the other hand, we have found only two experimental
papers in which the relevance of the residues is taken into account
through their mutation for the SARS-1 (Subissi et al., 2014) and
SARS-2 (Biswal et al., 2021) NSP12-NSP7-NSP8 complex. Thus,
new studies are necessary to understand this complex better, and our
analysis could help to present new residues that could be relevant to
the complex.

Two major hotspots in NSP12 were found, formed by the residues
F415, E431, F440, and A443, and R331, K332, L387, L388, and L389.
Our data suggest that designing an inhibitor for impairing the contacts
between the residues in the interface $NSP12$-$NSP8_1$ could be more
interesting than $NSP12$-$NSP8_2$, albeit NSP12-NSP7 could also be an
option, mainly in the regions shown in Figures 4, 7A. Finally, the
introduction of RNA+remdesivir in the complex almost does not alter
the IE of the residue-residue pairs of NSP12-NSP7, while changes are
more evident in $NSP12$-$NSP8_1$. These results provide valuable
information for the discovery of antiviral therapeutics that inhibit
these protein-protein interactions in human pathogenic CoVs.

Data availability statement

The original contributions presented in the study are included in
the article/Supplementary Material, further inquiries can be directed
to the corresponding authors.

Author contributions

JL: Conceptualization, Writing–original draft. KS: Data
curation, Writing–original draft. ED: Methodology,
Writing–original draft. RA: Formal Analysis, Writing–original
draft. DG: Formal Analysis, Writing–original draft. ML:

Validation, Writing–original draft. JN: Visualization, Writing–original draft. SA: Investigation, Writing–original draft. YB: Supervision, Writing–original draft. H-AN: Supervision, Writing–original draft. MB: Writing–original draft, Writing–review and editing. UF: Formal Analysis, Writing–original draft.

Funding

Acknowledgments

Conflict of interest

The authors declare that the research was conducted in the absence of any commercial or financial relationships that could be construed as a potential conflict of interest.

Publisher's note

All claims expressed in this article are solely those of the authors and do not necessarily represent those of their affiliated organizations, or those of the publisher, the editors and the reviewers. Any product that may be evaluated in this article, or claim that may be made by its manufacturer, is not guaranteed or endorsed by the publisher.

Supplementary material

The Supplementary Material for this article can be found online at: https://www.frontiersin.org/articles/10.3389/fmolb.2023.1325588/full#supplementary-material

References

Aggarwal, A., Naskar, S., Maroli, N., Gorai, B., Dixit, N. M., and Maiti, P. K. (2021). Mechanistic insights into the effects of key mutations on SARS-CoV-2 RBD–ACE2 binding. *Phys. Chem. Chem. Phys.* 23 (46), 26451–26458. doi:10.1039/D1CP04005G

Albuquerque, E. L., Fulco, U. L., Caetano, E. W., and Freire, V. N. (2021). *Quantum chemistry simulation of biological molecules*. Cambridge University Press. Oxford/UK.

Amaral, J. L., Oliveira, J. T. A., Lopes, F. E. S., Freitas, C. D. T., Freire, V. N., Abreu, L. V., et al. (2022). Quantum biochemistry, molecular docking, and dynamics simulation revealed synthetic peptides induced conformational changes affecting the topology of the catalytic site of SARS-CoV-2 main protease. *J. Biomol. Struct. Dyn.* 40 (19), 8925–8937. doi:10.1080/07391102.2021.1920464

Anderson, A. S., Caubel, P., Rusnak, J. M., and EPIC-HR Trial Investigators (2022). Nirmatrelvir–ritonavir and viral load rebound in COVID-19. *N. Engl. J. Med.* 387 (11), 1047–1049. doi:10.1056/NEJMc2205944

Anjum, F., Mohammad, T., Asrani, P., Shafie, A., Singh, S., Yadav, D. K., et al. (2022). Identification of intrinsically disorder regions in non-structural proteins of SARS-CoV-2: new insights into drug and vaccine resistance. *Mol. Cell. Biochem.* 477 (5), 1607–1619. doi:10.1007/s11010-022-04393-5

Bagabir, S. A. (2023). Investigating the potential of natural compounds as novel inhibitors of SARS-CoV-2 RdRP using computational approaches. *Biotechnol. Genet. Eng. Rev.* 2023, 1–21. doi:10.1080/02648725.2023.2195240

Barone, V., and Cossi, M. (1998). Quantum calculation of molecular energies and energy gradients in solution by a conductor solvent model. *J. Phys. Chem. A* 102 (11), 1995–2001. doi:10.1021/jp9716997

Bezerra, K. S., Fulco, U. L., Esmaile, S. C., Lima Neto, J. X., Machado, L. D., Freire, V. N., et al. (2019). Ribosomal RNA–aminoglycoside hygromycin b interaction energy calculation within a density functional theory framework. *J. Phys. Chem. B* 123 (30), 6421–6429. doi:10.1021/acs.jpcb.9b04468

Bezerra, K. S., Vianna, J. F., Lima Neto, J. X., Ivan Nobre Oliveira, J., Albuquerque, E. L., and Fulco, U. L. (2020). Interaction energies between two antiandrogenic and one androgenic agonist receptor in the presence of a T877A mutation in prostate cancer: a quantum chemistry analysis. *New J. Chem.* 44 (15), 5903–5912. doi:10.1039/C9NJ06276A

Biovia Dassault Systèmes (2021). *Discovery studio visualizer*. San Diego, CA, USA: Dassault Systèmes, 2021.

Biswal, M., Diggs, S., Xu, D., Khudaverdyan, N., Lu, J., Fang, J., et al. (2021). Two conserved oligomer interfaces of NSP7 and NSP8 underpin the dynamic assembly of SARS-CoV-2 RdRP. *Nucleic Acids Res.* 49 (10), 5956–5966. doi:10.1093/nar/gkab370

Biswas, N., Kumar, K., Mallick, P., Das, S., Kamal, I. M., Bose, S., et al. (2021). Structural and drug screening analysis of the non-structural proteins of severe acute respiratory syndrome coronavirus 2 virus extracted from Indian coronavirus disease 2019 patients. *Front. Genet.* 12, 626642. doi:10.3389/fgene.2021.626642

Bogan, A. A., and Thorn, K. S. (1998). Anatomy of hot spots in protein interfaces. *J. Mol. Biol.* 280 (1), 1–9. doi:10.1006/jmbi.1998.1843

Burley, S. K., Berman, H. M., Bhikadiya, C., Bi, C., Chen, L., Di Costanzo, L., et al. (2019). RCSB Protein Data Bank: biological macromolecular structures enabling research and education in fundamental biology, biomedicine, biotechnology and energy. *Nucleic Acids Res.* 47 (D1), D464–D474. doi:10.1093/nar/gky1004

Butler, C. C., Hobbs, F. D. R, Gbinigie, O. A., Rahman, N. M., Hayward, G., Richards, D. B., et al. (2023). Molnupiravir plus usual care versus usual care alone as early treatment for adults with COVID-19 at increased risk of adverse outcomes (PANORAMIC): an open-label, platform-adaptive randomised controlled trial. *Lancet* 401 (10373), 281–293. doi:10.1016/S0140-6736(22)02597-1

Campos, D. M. O., Bezerra, K. S., Esmaile, S. C., Fulco, U. L., Albuquerque, E. L., and Oliveira, J. I. N. (2020). Intermolecular interactions of cn-716 and acyl-KR-aldehyde dipeptide inhibitors against zika virus. *Phys. Chem. Chem. Phys.* 22 (27), 15683–15695. doi:10.1039/D0CP02254C

Charness, M. E., Gupta, K., Stack, G., Strymish, J., Adams, E., Lindy, D. C., et al. (2022). Rebound of SARS-CoV-2 infection after nirmatrelvir–ritonavir treatment. *N. Engl. J. Med.* 387 (11), 1045–1047. doi:10.1056/NEJMc2206449

Consortium, W. S. T., Pan, H., Peto, R., Henao-Restrepo, A. M., Preziosi, M. P., Sathiyamoorthy, V., et al. (2021). Repurposed antiviral drugs for COVID-19–interim WHO solidarity trial results. *N. Engl. J. Med.* 384 (6), 497–511. doi:10.1056/NEJMoa2023184

Cossi, M., Rega, N., Scalmani, G., and Barone, V. (2003). Energies, structures, and electronic properties of molecules in solution with the c-PCM solvation model. *J. Comput. Chem.* 24 (6), 669–681. doi:10.1002/jcc.10189

Cox, M., Peacock, T. P., Harvey, W. T., Hughes, J., Wright, D. W., Willett, B. J., et al. (2023). SARS-CoV-2 variant evasion of monoclonal antibodies based on *in vitro* studies. *Nat. Rev. Microbiol.* 21 (2), 112–124. doi:10.1038/s41579-022-00809-7

Cukuroglu, E., Engin, H. B., Gursoy, A., and Keskin, O. (2014). Hot spots in protein–protein interfaces: towards drug discovery. *Prog. Biophys. Mol. Biol.* 116 (2–3), 165–173. doi:10.1016/j.pbiomolbio.2014.06.003

da Costa, R. F., Freire, V. N., Bezerra, E. M., Cavada, B. S., Caetano, E. W. S., de Lima Filho, J. L., et al. (2012). Explaining statin inhibition effectiveness of HMG-CoA reductase by quantum biochemistry computations. *Phys. Chem. Chem. Phys.* 14 (4), 1389–1398. doi:10.1039/C1CP22824B

de Oliveira, F. L. S, Vieira Carletti, J., Azevedo, F. F. N., Freitas de Sousa, F. J., Caetano, E. W. S., Freire, V. N., et al. (2020). mTOR–mLST8 interaction: hot spot identification through quantum biochemistry calculations. *New J. Chem.* 44 (48), 20982–20992. doi:10.1039/D0NJ04099A

De Sousa, B. G., Oliveira, J. I. N., Albuquerque, E. L., Fulco, U. L., Amaro, V. E., and Blaha, C. A. G. (2017). Molecular modelling and quantum biochemistry computations of a naturally occurring bioremediation enzyme: alkane hydroxylase from

Pseudomonas putida P1. *J. Mol. Graph. Model.* 77, 232–239. doi:10.1016/j.jmgm.2017.08.021

Elkarhat, Z., Charoute, H., Elkhattabi, L., Barakat, A., and Rouba, H. (2022). Potential inhibitors of SARS-cov-2 RNA dependent RNA polymerase protein: molecular docking, molecular dynamics simulations and MM-PBSA analyses. *J. Biomol. Struct. Dyn.* 40 (1), 361–374. doi:10.1080/07391102.2020.1813628

Ershov, P. V., Mezentsev, Y. V., and Ivanov, A. S. (2022). Interfacial peptides as affinity modulating agents of protein–protein interactions. *Biomolecules* 12 (1), 106. doi:10.3390/biom12010106

Frisch, M. J. (2016). *Gaussian 16*. Wallingford, CT: Gaussian, Inc.

Gao, Y., Yan, L., Huang, Y., Liu, F., Zhao, Y., Cao, L., et al. (2020). Structure of the RNA-dependent RNA polymerase from COVID-19 virus. *Science* 368 (6492), 779–782. doi:10.1126/science.abb7498

Giannetti, M., Mazzuca, C., Ripani, G., and Palleschi, A. (2023). Inspection on the mechanism of SARS-CoV-2 inhibition by penciclovir: a molecular dynamic study. *Molecules* 28 (1), 191. doi:10.3390/molecules28010191

Grimme, S. (2006). Semiempirical GGA-type density functional constructed with a long-range dispersion correction. *J. Comput. Chem.* 27 (15), 1787–1799. doi:10.1002/jcc.20495

Gu, Y., Liu, M., Staker, B. L., Buchko, G. W., and Quinn, R. J. (2023). Drug-repurposing screening identifies a gallic acid binding site on SARS-CoV-2 non-structural protein 7. *ACS Pharmacol. Transl. Sci.* 6, 578–586. doi:10.1021/acsptsci.2c00225

Harvey, W. T., Carabelli, A. M., Jackson, B., Gupta, R. K., Thomson, E. C., Harrison, E. M., et al. (2021). SARS-CoV-2 variants, spike mutations and immune escape. *Nat. Rev. Microbiol.* 19 (7), 409–424. doi:10.1038/s41579-021-00573-0

He, X., Zhu, T., Wang, X., Liu, J., and Zhang, J. Z. (2014). Fragment quantum mechanical calculation of proteins and its applications. *Acc. Chem. Res.* 47 (9), 2748–2757. doi:10.1021/ar500077t

Iketani, S., Mohri, H., Culbertson, B., Hong, S. J., Duan, Y., Luck, M. I., et al. (2023). Multiple pathways for SARS-CoV-2 resistance to nirmatrelvir. *Nature* 613 (7944), 558–564. doi:10.1038/s41586-022-05514-2

Kabinger, F., Stiller, C., Schmitzová, J., Dienemann, C., Kokic, G., Hillen, H. S., et al. (2021). Mechanism of molnupiravir-induced SARS-CoV-2 mutagenesis. *Nat. Struct. Mol. Biol.* 28 (9), 740–746. doi:10.1038/s41594-021-00651-0

Kirchdoerfer, R. N., and Ward, A. B. (2019). Structure of the SARS-CoV NSP12 polymerase bound to NSP7 and NSP8 co-factors. *Nat. Commun.* 10 (1), 2342–2349. doi:10.1038/s41467-019-10280-3

Kobryn, A. E., Maruyama, Y., Velazquez-Martinez, C. A., Yoshida, N., and Gusarov, S. (2021). Modeling the interaction of SARS-CoV-2 binding to the ACE2 receptor via molecular theory of solvation. *New J. Chem.* 45 (34), 15448–15457. doi:10.1039/D1NJ02015C

Lima Neto, J. X., Bezerra, K. S., Barbosa, E. D., Oliveira, J. I. N., Manzoni, V., Soares-Rachetti, V. P., et al. (2019). Exploring the binding mechanism of GABAB receptor agonists and antagonists through *in silico* simulations receptor agonists and antagonists through *in silico* simulations. *J. Chem. Inf. Model.* 60 (2), 1005–1018. doi:10.1021/acs.jcim.9b01025

Lima Neto, J. X., Fulco, U. L., Albuquerque, E. L., Corso, G., Bezerra, E. M., Caetano, E. W. S., et al. (2015). A quantum biochemistry investigation of willardiine partial agonism in AMPA receptors. *Phys. Chem. Chem. Phys.* 17 (19), 13092–13103. doi:10.1039/C4CP05630B

Lima Neto, J. X., Soares-Rachetti, V. P., Albuquerque, E. L., Manzoni, V., and Fulco, U. L. (2018). Outlining migrainous through dihydroergotamine–serotonin receptor interactions using quantum biochemistry. *New J. Chem.* 42 (4), 2401–2412. doi:10.1039/C7NJ03645K

Lima Neto, J. X., Vieira, D. S., de Andrade, J., and Fulco, U. L. (2022). Exploring the spike-hACE 2 residue–residue interaction in human coronaviruses SARS-CoV-2, SARS-CoV, and HCoV-NL63. *J. Chem. Inf. Model.* 62, 2857–2868. doi:10.1021/acs.jcim.1c01544

Liu, J., Wang, X., Zhang, J., and He, X. (2015). Calculation of protein-ligand binding affinities based on a fragment quantum mechanical method. *RSC Adv.* 5, 107020–107030. doi:10.1039/C5RA20185C

McCarthy, K. R., Rennick, L. J., Nambulli, S., Robinson-McCarthy, L. R., Bain, W. G., Haidar, G., et al. (2021). Recurrent deletions in the SARS-CoV-2 spike glycoprotein drive antibody escape. *Science* 371 (6534), 1139–1142. doi:10.1126/science.abf6950

Merz, K. M., Jr (2014). Using quantum mechanical approaches to study biological systems. *Acc. Chem. Res.* 47 (9), 2804–2811. doi:10.1021/ar5001023

Moghadasi, S. A., Heilmann, E., Khalil, A. M., Nnabuife, C., Kearns, F. L., Ye, C., et al. (2023). Transmissible SARS-CoV-2 variants with resistance to clinical protease inhibitors. *Sci. Adv.* 9 (13), eade8778. doi:10.1126/sciadv.ade8778

Momany, F. A., and Rone, R. (1992). Validation of the general purpose QUANTA ®3.2/CHARMm® force field. *J. Comput. Chem.* 13 (7), 888–900. doi:10.1002/jcc.540130714

Morais, P. A., Maia, F. F., Solis-Calero, C., Caetano, E. W. S., Freire, V. N., and Carvalho, H. F. (2020). The urokinase plasminogen activator binding to its receptor: a quantum biochemistry description within an in/homogeneous dielectric function

framework with application to uPA–uPAR peptide inhibitors. *Phys. Chem. Chem. Phys.* 22 (6), 3570–3583. doi:10.1039/C9CP06530J

Mutlu, O., Ugurel, O. M., Sariyer, E., Ata, O., Inci, T. G., Ugurel, E., et al. (2022). Targeting SARS-CoV-2 Nsp12/Nsp8 interaction interface with approved and investigational drugs: an *in silico* structure-based approach. *J. Biomol. Struct. Dyn.* 40 (2), 1–13. doi:10.1080/07391102.2020.1819882

Narayanan, A., Narwal, M., Majowicz, S. A., Varricchio, C., Toner, S. A., Ballatore, C., et al. (2022). Identification of SARS-CoV-2 inhibitors targeting mpro and PLpro using in-cell-protease assay. *Commun. Biol.* 5 (1), 169–217. doi:10.1038/s42003-022-03090-9

Padhi, A. K., Shukla, R., Saudagar, P., and Tripathi, T. (2021). High-throughput rational design of the remdesivir binding site in the RdRp of SARS-CoV-2: implications for potential resistance. *Iscience* 24 (1), 101992. doi:10.1016/j.isci.2020.101992

Peng, Q., Peng, R., Yuan, B., Zhao, J., Wang, M., Wang, X., et al. (2020). Structural and biochemical characterization of the nsp12-nsp7-nsp8 core polymerase complex from SARS-CoV-2. *Cell Rep.* 31 (11), 107774. doi:10.1016/j.celrep.2020.107774

Pereira, A., Bezerra, K., Santos, J., Oliveira, J. I., Freire, V., and Fulco, U. (2021). *In silico* approach of modified melanoma peptides and their immunotherapeutic potential. *Phys. Chem. Chem. Phys.* 23 (4), 2836–2845. doi:10.1039/d0cp05322h

Raha, K., Peters, M. B., Wang, B., Yu, N., Wollacott, A. M., Westerhoff, L. M., et al. (2007). The role of quantum mechanics in structure-based drug design. *Drug Discov. Today* 12 (17–18), 725–731. doi:10.1016/j.drudis.2007.07.006

Reshamwala, S. M., Likhite, V., Degani, M. S., Deb, S. S., and Noronha, S. B. (2021). Mutations in SARS-CoV-2 nsp7 and nsp8 proteins and their predicted impact on replication/transcription complex structure. *J. Med. Virol.* 93 (7), 4616–4619. doi:10.1002/jmv.26791

Rodrigues, C., Oliveira, J., Fulco, U., Albuquerque, E., Moura, R., Caetano, E., et al. (2013). Quantum biochemistry study of the T3-785 tropocollagen triple-helical structure. *Chem. Phys. Lett.* 559, 88–93. doi:10.1016/j.cplett.2012.12.061

Ruan, Z., Liu, C., Guo, Y., He, Z., Huang, X., Jia, X., et al. (2021). SARS-CoV-2 and SARS-CoV: virtual screening of potential inhibitors targeting RNA-dependent RNA polymerase activity (NSP12). *J. Med. Virol.* 93 (1), 389–400. doi:10.1002/jmv.26222

Ryde, U., and Söderhjelm, P. (2016). Ligand-binding affinity estimates supported by quantum-mechanical methods. *Chem. Rev.* 116 (9), 5520–5566. doi:10.1021/acs.chemrev.5b00630

Santos, J. L. S., Bezerra, K. S., Barbosa, E. D., Pereira, A. C. L., Meurer, Y. S. R., Oliveira, J. I. N., et al. (2022). *In silico* analysis of energy interactions between nociceptin/orfanin FQ receptor and two antagonists with potential antidepressant action. *New J. Chem.* 46 (17), 7950–7959. doi:10.1039/D2NJ00916A

Sarma, H., Jamir, E., and Sastry, G. N. (2022). Protein-protein interaction of RdRp with its co-factor NSP8 and NSP7 to decipher the interface hotspot residues for drug targeting: a comparison between SARS-CoV-2 and SARS-CoV. *J. Mol. Struct.* 1257, 132602. doi:10.1016/j.molstruc.2022.132602

Scott, D. E., Bayly, A. R., Abell, C., and Skidmore, J. (2016). Small molecules, big targets: drug discovery faces the protein–protein interaction challenge. *Nat. Rev. Drug Discov.* 15 (8), 533–550. doi:10.1038/nrd.2016.29

Silva, S. R. B., Lima Neto, J. X., Fuzo, C. A., Fulco, U. L., and Vieira, D. S. (2020). A quantum biochemistry investigation of the protein-protein interactions for the description of allosteric modulation on biomass-degrading chimera. *Phys. Chem. Chem. Phys.* 22 (44), 25936–25948. doi:10.1039/D0CP04415F

Søndergaard, C. R., Olsson, M. H., Rostkowski, M., and Jensen, J. H. (2011). Improved treatment of ligands and coupling effects in empirical calculation and rationalization of pKa values. *J. Chem. Theory Comput.* 7 (7), 2284–2295. doi:10.1021/ct200133y

Subissi, L., Posthuma, C. C., Collet, A., Zevenhoven-Dobbe, J. C., Gorbalenya, A. E., Decroly, E., et al. (2014). One severe acute respiratory syndrome coronavirus protein complex integrates processive RNA polymerase and exonuclease activities. *Proc. Natl. Acad. Sci. U.S.A.* 111 (37), E3900–E3909. doi:10.1073/pnas.1323705111

Tavares, A. B. M., Lima Neto, J., Fulco, U., and Albuquerque, E. (2021). Blockade of the checkpoint PD-1 by its ligand PD-L1 and the immuno-oncological drugs pembrolizumab and nivolumab. *Phys. Chem. Chem. Phys.* 23 (37), 21207–21217. doi:10.1039/D1CP03064G

Tavares, A. B. M., Lima Neto, J. X., Fulco, U. L., and Albuquerque, E. L. (2018). Inhibition of the checkpoint protein PD-1 by the therapeutic antibody pembrolizumab outlined by quantum chemistry. *Sci. Rep.* 8 (1), 1840–1913. doi:10.1038/s41598-018-20325-0

Tian, L., Qiang, T., Liang, C., Ren, X., Jia, M., Zhang, J., et al. (2021). RNA-dependent RNA polymerase (RdRp) inhibitors: the current landscape and repurposing for the COVID-19 pandemic. *Eur. J. Med. Chem.* 213, 113201. doi:10.1016/j.ejmech.2021.113201

Vianna, J. F., Bezerra, K. S., Lima Costa, A. H., Barbosa, E. D., Lima Neto, J. X., Oliveira, J. I. N., et al. (2021). New ethionamide boosters and EthR2: structural and energetic analysis. *Phys. Chem. Chem. Phys.* 23 (40), 23233–23241. doi:10.1039/D1CP02853G

Vicatos, S., Roca, M., and Warshel, A. (2009). Effective approach for calculations of absolute stability of proteins using focused dielectric constants. *Proteins* 77 (3), 670–684. doi:10.1002/prot.22481

Wilamowski, M., Hammel, M., Leite, W., Zhang, Q., Kim, Y., Weiss, K. L., et al. (2021). Transient and stabilized complexes of Nsp7, Nsp8, and Nsp12 in SARS-CoV-2 replication. *Biophys. J.* 120 (15), 3152–3165. doi:10.1016/j.bpj.2021.06.006

World Health Organization (2020). WHO coronavirus (COVID-19) dashboard. Available at: https://covid19.who.int/ (Accessed July 6, 2023).

Yadav, R., Chaudhary, J. K., Jain, N., Chaudhary, P. K., Khanra, S., Dhamija, P., et al. (2021). Role of structural and non-structural proteins and therapeutic targets of SARS-CoV-2 for COVID-19. *Cells* 10 (4), 821. doi:10.3390/cells10040821

Yin, W., Mao, C., Luan, X., Shen, D. D., Shen, Q., Su, H., et al. (2020). Structural basis for inhibition of the RNA-dependent RNA polymerase from

SARS-CoV-2 by remdesivir. *Science* 368 (6498), 1499–1504. doi:10.1126/science.abc1560

Zhai, J., He, X., Man, V. H., Sun, Y., Ji, B., Cai, L., et al. (2022). A multiple-step *in silico* screening protocol to identify allosteric inhibitors of spike–hACE2 binding. *Phys. Chem. Chem. Phys.* 24 (7), 4305–4316. doi:10.1039/D1CP04736A

Zhang, D. W., and Zhang, J. (2003). Molecular fractionation with conjugate caps for full quantum mechanical calculation of protein–molecule interaction energy. *J. Chem. Phys.* 119 (7), 3599–3605. doi:10.1063/1.1591727

Zhou, T., Huang, D., and Caflisch, A. (2010). Quantum mechanical methods for drug design. *Curr. Top. Med. Chem.* 10 (1), 33–45. doi:10.2174/156802610790232242